RSC Advances

ROYAL SOCIETY OF CHEMISTRY

www.rsc.org/advances

RSC Advances

ARTICLE

Enhanced electrical and luminescent performance of porous silicon/MEH-PPV nanohybrid synthesized by anodization and repeated spin coating

Received 00th January 20xx,
Accepted 00th January 20xx

DOI: 10.1039/x0xx00000x

www.rsc.org/

A. M. S. Salem,[a] F. A. Harraz,[a,†] S. M. El-Sheikh,[a] H. S. Hafez,[b] I. A. Ibrahim[a] and M. S. A. Abdel Mottaleb[c]

The electrochemical anodization of a single crystalline silicon in hydrofluoric acid-based solution leads to the formation of porous silicon (PSi) of tunable pore size and morphology for a wide range of technological applications. By infiltrating the as-anodized PSi layer with conducting polymer, new functionalities can be achieved. Herein, we report on the enhancement of the electrical and luminescent properties of a nanohybrid composed of ~100 nm PSi infiltrated by poly(2-methoxy-5-(2-ethylhexyloxy)-*p*-phenylenevinylene) (MEH-PPV) via a repeated spin coating technique. Morphological and structural investigations using FE-SEM and XRD of the hybrid nanostructure revealed a successful deposition of MEH-PPV inside the entire porous channels with a low degree of crystallinity. A partial silicon oxide formation was confirmed by FT-IR and XPS measurements. Furthermore, a remarkable increase in the electrical properties was detected by measuring the *I-V* curves and the electrochemical impedance spectroscopy (EIS). Moreover, a noticeable photoluminescence (PL) spectral enhancement after the MEH-PPV deposition into the PSi was detected. The spectral analyses for the current system indicate the possibility of exciton transfer from PSi to MEH-PPV polymer. This simple synthetic approach can open new opportunities for the development of hybrid nanostructures of PSi and conducting polymers with potential for optical device applications.

1. Introduction

The research fields of conducting polymers and nanostructured silicon scaffolds, particularly porous silicon (PSi) had been rapidly developing over the past decade[1-3]. Essentially, conducting polymers exhibit distinctive features such as lightweight, flexibility, ease of processing, and unique electrical and photonic charactarestics[4,,5]. The combination of the two components (organic-inorganic) into a single hybrid system could lead to desirable physicochemical properties that would open exciting opportunities for fabricating advanced functional materials[6-11]. Such organic based nanocomposites have been extensively studied for photo- and electro-responsive devices, including photodetectors, light-emitting diodes, and photovoltaic devices [12-14].

The discovery of the room temperature visible photoluminescence (PL) and electroluminescence (EL) of porous silicon (PSi) has stimulated an enormous interest owning to its potential application in solar cells, light emitting diodes, chemical and bio-sensors, interference filters, waveguide, silicon-on-insulator (SOI) structures, and biomedical applications, etc. [15] Specially, this luminescence property has not been observed in bulk silicon[16]. Therefore, several research groups have investigated the properties of hybrid composite materials of PSi layer with conducting polymers[17-19], including Poly[2-methoxy-5-(2-ethylhexyloxy)-1,4-phenylenevinylene] (MEH-PPV) [20].

Spin casting has become one of the most commonly used techniques for obtaining uniform thin films[11]. Baltchford *et al.* [21] have observed that the polymeric films that are cast with different solvents exhibited different PL spectral responses. This observation implies that the morphology or the aggregation of polymer chains has a remarkable effect on final emission spectra. In continuation of our previous works[22-25], herein we report the infiltration of MEH-PPV conducting polymer into the pores of PSi via a simple spin coating technique. MEH-PPV is dissolved in different organic solvents, followed by infiltration into the pores of PSi. The detailed of the experimental approach, along with the electrical and optical properties of the prepared nanohybrids are thoroughly addressed and discussed.

2. Experimental

2.1. Materials

[a] *Nanostructured Materials and Nanotechnology Division, Central Metallurgical Research and Development Institute (CMRDI),P.O. Box: 87 Helwan, Cairo 11421 Egypt.*
[b] *Environmental Studies and Research Institute, Sadat University, Sadat City, Egypt.*
[c] *Nano-Photochemistry and Solar Chemistry Labs., Department of Chemistry, Faculty of Science, Ain Shams University, Abbassia, Cairo, Egypt.*
† E-mail: fharraz68@yahoo.com; Tel: +20-27142452; Fax: +20-27142451
Electronic Supplementary Information (ESI) available: [details of any supplementary information available should be included here]. See DOI: 10.1039/x0xx00000x

HF, $KMnO_4$, DMSO, TBAP, acetone, MEH-PPV (average M_n 40,000-70,000), chloroform, THF and toluene were purchased from Sigma-Aldrich (St. Louis, MO, USA), and used as received without further treatment.

2.2. Formation of PSi template

Porous silicon (PSi) templates were fabricated in *n*-type Si, according to our previous procedures [22-24], by a galvanostatic anodization in 6 wt.% HF in the presence of 8 mM $KMnO_4$ as oxidizing agent and NCW-1001 as a surfactant (Wako Pure Chemical Ind.). For macropores, *p*-type Si was anodized in 6 wt.% HF in the presence of dimethyl sulfoxide (DMSO) as an organic solvent and tetra-n-butylammonium perchlorate (TBAP) as a supporting electrolyte. To remove the native oxide from the surface of Si wafer before the formation of PSi, the Si wafer was immersed in acetone with ultrasonication for 10 min, followed by rinsing in 5 wt.% aqueous HF. The electrochemical etching was conducted in a two-electrode set up with 0.78 cm^2 Si working electrode and a Pt rod served as a counter electrode. The anodization process was performed with applied current densities of 20 and 10 mA/cm^2 for 300 s, producing pore arrays with sizes of ~100 nm and 2 µm, respectively. The PSi formation was conducted under computer control using a Potentiostat/Galvanostat /FRA, model 2273 of the Princeton Applied Research.

2.3. Spin coating of MEH-PPV into PSi template

The spin coating was conducted on the wet porous layer after rinsing in ethanol. MEH-PPV solution was prepared by dissolving 0.025 g of MEH-PPV in 100 ml of various organic solvents; mainly chloroform, tetrahydrofuran (THF) and Toluene. The MEH-PPV powder was dissolved in the mentioned organic solvents and sonicated for enough time to ensure a homogeneous polymeric solution (HPS). Prior to spin coating, a delay time of 30 s was applied for efficient solvent infiltration into the porous structure due to capillarity. Then, few drops of (HPS) are placed on the front PSi template surface, and by using spin coating technique it could be infiltrated into the PSi channels. The porous layer was spun at 2000 rpm for 60 s and the spin coating was repeated on the wet substrate for 5 times in the case of 100 nm pore sizes, and for 10 cycles for the macropores. After that, the PSi containing MEH-PPV polymer was dried at 100 °C for 1 h. The films were then stored in the dark at room temperature to prevent photodegradation.

2.4. Characterization of PSi/MEH-PPV hybrid structure

Morphological investigation for as-formed hybrid structure was taken on field emission-scanning electron microscopy FE-SEM (FEG250-Quanta instrument) on the cleaved samples. Surface analysis was analyzed using thin film X-ray diffraction (XRD; PANalytical-x'pert pro, Netherland) equipped with nickel filters using Cu-Kα (λ= 1.5406 Å) as a source of radiation. Surface chemical composition of the MEH-PPV/PSi was investigated by X-ray Photoelectron Spectroscopy (XPS, England). Thermo-Scientific K-Alpha XPS system with X-ray source–Al Ka micro-focused monochromator–Variable spot size (30-400 ⍰m in 5 ⍰m steps), Ion Gun–Energy range 100-4000 eV, Vacuum System–2x 220 l/s turbo molecular pumps for entry & analysis chambers–Auto-firing, 3 filament TSP was employed. The binding energies were calibrated to the C1s peak at 284.4 eV of the surface adventitious carbon taken as a reference. A JASCO FT-IR-6300 pulse (Japan) was used to record Fourier transform infrared (FT-IR) spectra. To improve the signal-to-noise ratio, each spectrum is taken as the average of 64 scans, with 4 cm^{-1} resolution. The spectrum of a Si wafer preliminarily treated with 5 wt.% aqueous HF was used as a reference. The electrochemical measurements including the electrochemical impedance spectroscopy (EIS) and the current-voltage (*I-V*) curves were measured using ZahnerZennium electrochemical workstation with Thales software. Room temperature photoluminescence (PL) for polymer solution as well as hybrid structures was measured by means of Spectrofluorophotometer, (RF-5301 PC, Japan, SHIMADZU, 400 W, 50/60 Hz) using a 150 W xenon lamp excitation source and 300 nm as an excitation wavelength.

3. Results and discussion

3.1. Morphological and structural properties

Figure 1a,b shows, respectively the FE-SEM micrographs of as-formed medium-sized pores with ~100 nm pore diameter and ~2 µm macropores of PSi templates before polymer infiltration. Figure 1c,d shows FE-SEM images with different magnifications for MEH-PPV deposited into ~100 nm pore diameter of PSi by the spin coating technique using toluene solution. While, Fig. 1e displays the deposition of MEH-PPV into ~2 µm macropores. MEH-PPV was successfully infiltrated inside the pores and coated the entire surface as well as the pore walls. Under the current spin coating conditions, the infiltration of the polymeric solution into the porous template was certainly enhanced. Without using spin coating, the drop casting alone could not efficiently allow the MEH-PPV solution to penetrate into the pores; even there is a difference in surface energy between the polymeric solution and the PSi substrate[26]. In case of macropores, the MEH-PPV multilayer coated the pore channel surface of the PSi layer is clearly observable from the corresponding cross-sectional image of Figure 1e. A successful infiltration of polypyrrole using the electro-oxidative polymerization of parent pyrrole monomers in acetonitrile solution into the PSi template has been also reported in our previous work[25].

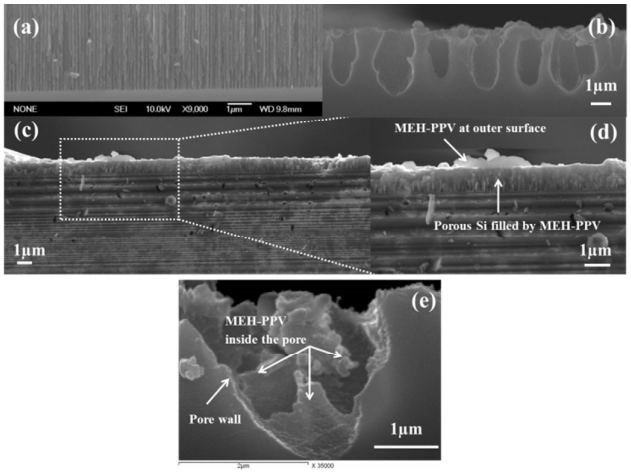

Fig. 1 (a) Cross-sectional view SEM images of as-formed medium-sized pores of ~100 nm; (b) as-formed macropores of ~2 µm; (c) MEH-PPV deposited into ~100 nm pore diameter of porous silicon by the spin coating technique (5 times) from toluene solution; (d) A magnification part of image (c); and (e) MEH-PPV spin coated into the macropores for 10 repeated cycles.

Figure 2 shows the XRD spectra of MEH-PPV films spin coated into PSi using THF, toluene and chloroform as organic solvents, along with the pattern measured for bare PSi. The hybrid structures exhibit broad diffraction peaks at 2θ=21.1° and large background indicating inhomogeneity of a short-range MEH-PPV chain arrangement. In a recent report, Urbánek *et al.* [27] have investigated the structural ordering as a function of MEH-PPV film thickness using XRD. Their results revealed that the development of a more ordered phase could be observed above a polymer thickness of 150 nm. Our observation indicates again that the crystallinity degree for the polymeric films prepared in all solvents is low and is hardily evaluated. The MEH-PPV polymeric chain is likely confined inside the porous template, which in turn alters its molecular structure to behave as an elongated and aligned chain segment. Another possibility for the appearance of such broad diffraction peaks after the polymer infiltration is the formation of Si oxide layer. This broad peak was not detected for the as-formed PSi, indicating the absence of native oxide layer in bare PSi. To confirm the formation of Si oxide after polymer deposition, further surface analysis using FTIR and XPS is conducted in the following sections.

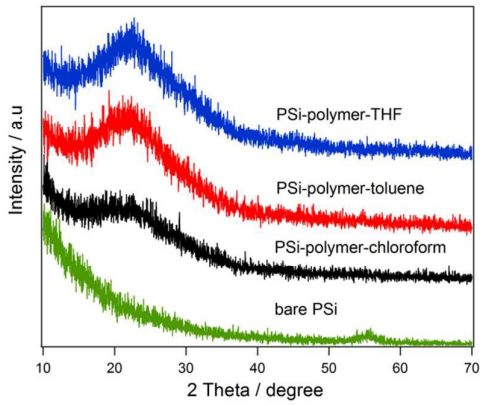

Fig. 2 X-ray diffraction patterns of bare porous silicon and MEH-PPV spin coated into porous silicon in different organic solvents.

Figure 3 represents the FT-IR spectra measured between 400-4000 cm^{-1} for the MEH-PPV in toluene solution and spin coated MEH-PPV film into PSi. The spectrum of as-formed PSi before polymer infiltration is also shown. The assignments of the absorption bands were done according to earlier work[28]. The characteristic peaks of the MEH-PPV conducting polymer as well as the complete assignments of the bands are listed in Table 1. It can be observed from the data listed in Table 1 that the bands position and type recorded from the toluene containing polymer are almost retained in the deposited MEH-PPV film. It is worth to note that the characteristic band of (RO)-CH_2 asymmetric vibration are observed at 1450 and 1457 cm^{-1} for the polymeric film and solution, respectively. The as-deposited MEH-PPV film reveals a band at 1736 cm^{-1} due to the formation of aromatic aldehyde (C-O stretch), which was also observed at 1732 cm^{-1} in the toluene solution. Moreover, the strong band appearing at 1108 cm^{-1} is assigned to Si-O-Si stretching mode appeared for PSi deposited polymeric film. In contrast to the as-formed polymeric film, the peaks at 3030 and 3432 cm^{-1} correspond, respectively to the –CH stretching vinyl and O-H stretching of the polymer solution. The absence of Si-O-Si stretching peak in bare PSi indicated the absence of native Si oxide layer in the freshly prepared sample. For more details, the FTIR spectra recorded for all polymeric solutions and for the deposited films into the PSi template using the three tested solvents (toluene, chloroform, THF) are presented as Supplementary Information (Fig.S1), along with a complete peak assignment collected in Table S1.

The XPS spectra of the MEH-PPV spin coated into PSi are shown in Fig. 4. The C1s and O1s photoelectron signals are investigated in both low resolution (survey) and high resolution indicating the presence of MEH-PPV polymer. The Si2p signal is also detected from the PSi template. The main Si2p, C1s, and O1s peaks are centered at ~99, 285, and 532 eV, respectively. However, it is noticed that the surface is partially oxidized in consistent with the above FT-IR observation (Fig.3). The Si2p spectrum exhibits two components: elemental Si (with oxidation state; Si (0) ~99 eV) and silicon oxide SiO_2 (with oxidation state; Si (4) ~103 eV[29]. It can be accordingly concluded from the FT-IR and XPS measurements that a partial oxidation of PSi takes place during the spin coating process and substrate drying, and thus a ternary system of PSi/SiO_2/MEH-PPV is likely obtained.

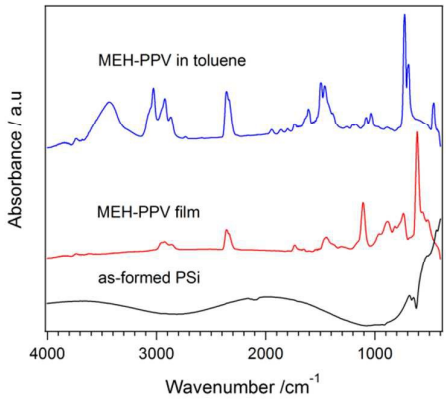

Fig. 3 FT-IR spectra recorded for MEH-PPV in toluene (top spectrum), spin coated MEH-PPV film into porous silicon (middle spectrum) and for bare porous silicon without polymer infiltration (bottom spectrum).

Table 1 FTIR peak assignments for MEH-PPV in toluene and as-formed film prepared by spin coating onto porous silicon.

Peak position (cm^{-1}), solution	Peak position (cm^{-1}) for deposited film	Peak assignments
3432	-	O-H stretching
3030	-	CH– stretching vinyl
-	2950	CH_3 antisymmetric stretching

2924	2924	CH– stretching
2865	2863	CH_2 stretching
1732	1736	Formation of aromatic aldehyde
1607	-	Aromatic stretching
1494	-	phenyl stretch (C-C aromatic)
1457	1450	Antisymmetric phenyl stretch
-	1108	Si-O-Si stretching
1033	-	Alkyl oxygen stretch
-	965	*Trans*-double bond CH-wag (vinyl group)
882	882	Out of plane phenyl CH-wag
727	736	Out of plane ring bend of phenyl ring

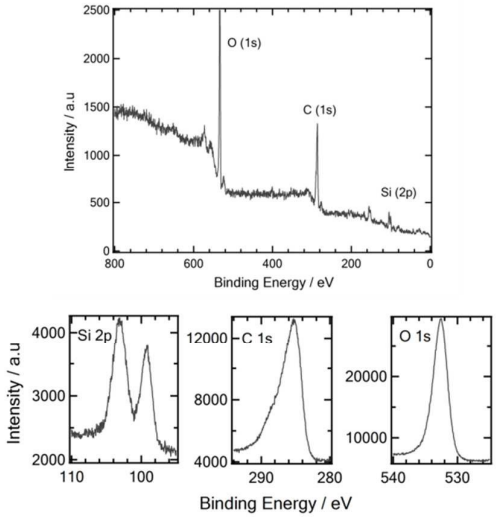

Fig. 4 XPS analysis of MEH-PPV spin coated into porous silicon from toluene solution; low resolution (top spectrum) and high resolution (bottom spectra).

3.2. Electrical properties

The electrical properties of the hybrid structure are measured. The samples received Ag backside contact using Ag past. Au is formed by sputtering through a mask onto the front side to establish an ohmic contact. The heterojunction diodes for as prepared PSi and MEH-PPV modified PSi have, respectively the following structures: Au/PSi/Ag and Au/MEH-PPV/PSi/Ag. The *I-V* characteristics for the above structures are shown in Fig. 5. It can be noticed that, the conductivity is greatly increased after spin coating the nanopores with conducting MEH-PPV polymer, indicating that the polymer would facilitate the transport of charge carriers inside the Si matrix. As a bulk effect, the enhancement of the conductivity is likely related to that the presence of conducting polymer inside the porous template would form efficient, conducting sites in the PSi structure which help to facilitate the transport of the charge carriers. The conductivity enhancement after polymer deposition indicated that the possibility for complete oxidation of PSi layer was excluded during polymer deposition.

The conductivity of hybrid structures of PSi/MEH-PPV is also evaluated by measuring the electrochemical impedance spectroscopy. The frequency dependence of the electrochemical impedance was measured in a wide range of 100 mHz to 100 kHz in the dark at 0.0 V for as-prepared PSi and PSi after MEH-PPV deposition. The result obtained for the Bode plot of EIS is depicted in Fig. 6. After polymer deposition (solid triangle: red curve) the electronic resistance and charge transfer resistance are found to increase compared to the PSi sample with no polymer deposition (empty triangle: blue curve). Similar behavior was observed using different applied potential mainly, 0.0, 0.2, 0.4, 0.6, and 0.8 V with respect to the open circuit potential (OCP) (data not shown). The enhancement of the electrical properties of the PSi template after polymer deposition is an indication that the MEH-PPV conducting polymer is successfully spin coated into the porous channels, with a small fraction of silicon being transformed to the insulating silicon dioxide as confirmed by FTIR and XPS measurements.

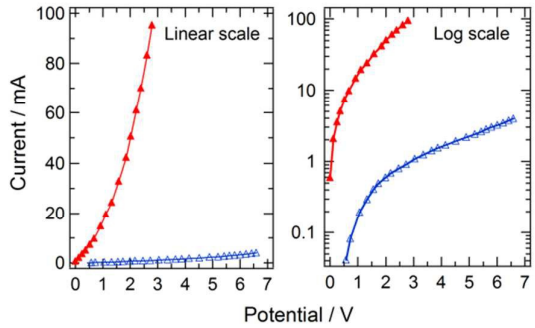

Fig. 5 *I–V* characteristics, measured in the dark, of the fabricated heterojunction plotted on a linear (left) and log scale (right). The red, solid triangles (▲) denote PSi diode with deposited MEH-PPV from toluene solution with a structure (Al/PSi/MEH-PPV/Au), whereas the blue, empty triangles (Δ) correspond to PSi without MEH-PPV polymer (Al/PSi/Au).

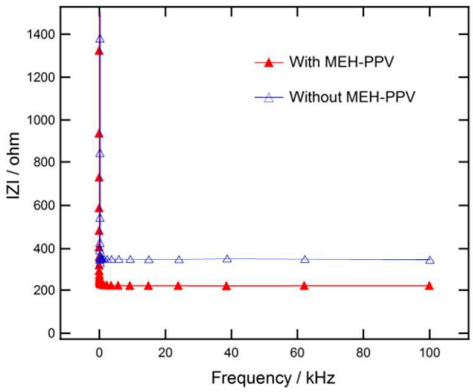

Fig. 6 Bode plot of EIS measured in the dark at 0.0 V *vs* Pt wire, in 0.1 M TBAP/CH_3CN for porous silicon without MEH-PPV and porous silicon with deposited MEH-PPV from toluene solution. The potential amplitude was 5 mV.

3.3. Photoluminescence for solutions and for solid films

The photoluminescence (PL) is firstly measured for MEH-PPV conducting polymer in toluene, chloroform and THF solvents. Figure

7 shows the PL emission spectra of MEH-PPV in a concentration of 0.25 mg/ml using the three above solvents measured at 300 nm excitation wavelength. As noted, emission peak is detected at 595 nm (2.08 eV) for MEH-PPV in toluene solution. Fluorescence emission spectral peaks are blue-shifted in case of chloroform and THF; emission peaks are located at 570 nm (2.18 eV) in both solvents. The emission blue shift observed for chloroform and THF solvents could, in principle, be related to the larger stabilization of the electronic ground sate of the MEH-PPV polymer in comparison with the stabilization of the electronic excited state [30].

Luminescence spectra of different concentrations of MEH-PPV in toluene solution (0.25, 0.50 and 1 mg/ml) are measured and the recorded spectra are depicted in Fig. 8. The PL spectrum obtained in 0.50 mg/ml concentrated solution (peak at 606 nm) is slightly red-shifted (11 nm) compared with the spectrum of sample with lower concentration (0.25 mg/ml). Further red-shift of ~16 nm was obtained upon increasing the concentration to 1 mg/ml. The results of Figs. 7 and 8 indicate that the PL spectral profile of MEH-PPV directly depends on solvent nature as well as the polymer concentration. Due to the difference in solvation ability of toluene, chloroform and THF, the solvents undergo different interactions with the polymer leading to different conformations with different energy levels in solutions that are reflected in the final PL properties.

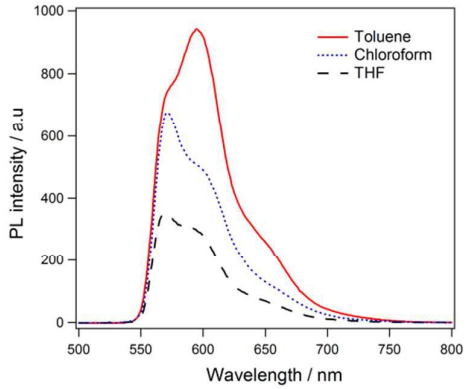

Fig. 7 Room temperature photoluminescence spectra of 0.25 mg/ml of MEH-PPV conducing polymer dissolved in toluene, chloroform and THF.

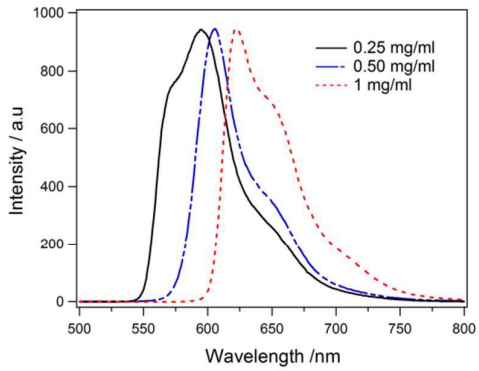

Fig. 8 Room temperature photoluminescence spectra of MEH-PPV measured in different concentrations of polymer in toluene: Concentrations: 0.25, 0.50 and 1 mg/ml.

According to the chemical structure of MEH-PPV, the structure consists of an aromatic polymer backbone and many ethyl-hexylyoxy side chains, and hence it is likely that aromatic solvents can solvate the polymer backbone better than the alkyl side chains. This is actually in agreement with what has been reported earlier that the toluene as an aromatic solvent undergoes a preferential solvation of the conjugated polymer backbone (vinylene-phenylene groups) inducing a more planer structure, whereas chloroform and THF likely undergo a preferential interaction with the lateral groups which led to a more flexible backbone[31]. The polymeric chains are accordingly solvated differently in toluene in one side compared to chloroform and THF on the other side. Upon preferential solvation of the backbone in toluene, good overlapping for the π-electrons with neighboring polymeric chains is expected. Increasing the polymer concentration led to much more segments that are available for interaction which resulted in an increase in the aggregation. The aggregation is promoted in toluene solution and hindered in chloroform and THF. The red-shift of the PL spectra could accordingly be related to: (i) the conformational changes of the polymer chain that modify the conjugation[32], (ii) the formation of aggregates that increases the relative intensity of the red-edge 0-1 vibronic band that has been reported to locate at 598 nm[31,33], very close to our PL emission peak observed in the current work.

Figure 9 shows the recorded PL spectra of MEH-PPV polymer films prepared by the spin coating into the PSi template in the previous mentioned solvents using a 0.25 mg/ml polymer concentration. Two important findings are observed, (i) the PL peak intensity of the structures after polymer coating are remarkably enhanced and slightly blue-shifted compared to the emission peak observed for bare PSi (with no polymer), and (ii) reference to the PL spectra of MEH-PPV measured in different solvents (Fig. 7) one can see a red-shift of the spectral profile for the spin-coated films with sharper peaks. In other words, the PL spectra of all nanohybrid structures of PSi and MEH-PPV (Fig. 9) are red-shifted and sharper compared with the spectra obtained in different solvents (Fig. 7). However, there is no great difference in the PL peak intensities for the three nanohybrids due to the polymer concentration used is very low where the polymeric chains have better conjugation in dilute solutions than in higher concentrations[34].

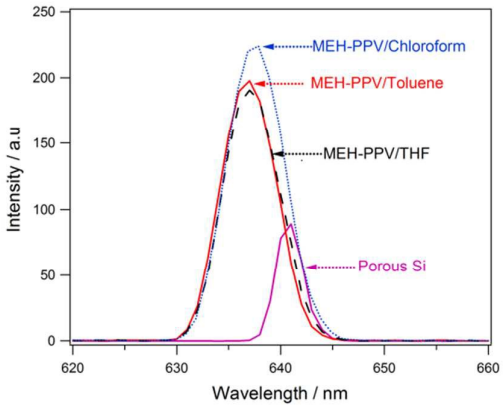

Fig. 9 Photoluminescence spectra of as-formed porous silicon and MEH-PPV films prepared by spin coating into porous silicon in different solvents: chloroform, toluene and THF. Spin coating conditions are in the text.

To better understand the PL spectral enhancement after the MEH-PPV deposition into the PSi and to test the possibility of excitation transfer from PSi to the polymer, we measured the UV-vis absorbance of the MEH-PPV film and compare the profile with the PL spectra of unmodified PSi layer. Figure 10 shows the UV-vis absorbance spectra of MEH-PPV (a) and the PL spectra of PSi (b). It is evident that MEH-PPV polymer had a significant absorption in the main PSi excited wavelength regime, due to the good overlapping with the luminescence energy band of PSi. As a result, the energy transfer from the PSi to MEH-PPV film is possible resulting in PL enhancement observed. The PL enhancement is consistent with the recent published work of electrochemically deposited a group of conducting polymers into meso-PSi templates[35]. Additionally, the polymer chains are confined inside the pores and being separated by the pore walls and hence their movement is restricted. This led to increase the polymer conjugation as the degree of collisions between polymer molecules is retarded[36], which in turn could enhance the emission of MEH-PPV conducting polymer.

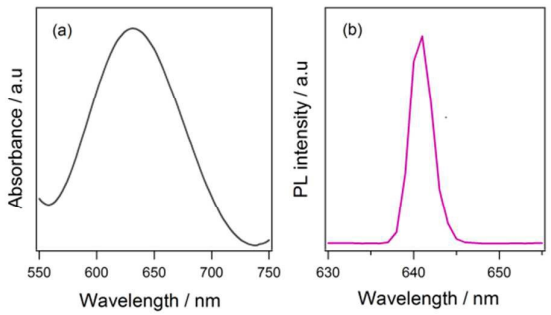

Fig. 10 UV-vis absorbance of MEH-PPV film (a) and photoluminescence spectrum of porous silicon (b). Adapted from our work[35].

4. Conclusions

In summary, hybrid nanostructures based on PSi layers (~100 nm pore sizes) and MEH-PPV polymer have been successfully fabricated by the electrochemical anodization of crystalline silicon, followed by repeated spin coating technique. The PSi layers were efficiently infiltrated with the polymer which displayed a low degree of crystallinity. Under the current fabrication conditions, a ternary system of PSi/SiO_2/MEH-PPV has been produced as elucidated by FT-IR and XPS. Significant increase in both electrical and luminescence properties of the nanohybrids could be clearly observed. The use of different organic solvents (chloroform, toluene, and THF) led to different interactions with MEH-PPV and generated different conformations in spin coating solutions, which finally affected the PL spectral responses of the hybrid structures. The obtained results imply that there is a great potential for such nanohybrids in current or future technologies such as optical devices, photovoltaic or sensing applications.

Acknowledgements

Research and instrumental facilities of Central Metallurgical Research and Development Institute (CMRDI) are acknowledged.

References

1 P. Reiss, E. Couderc, J. De Girolamo and A. Pron, *Nanoscale*, 2011, **3**, 446.
2 Polymer-Porous Silicon Composites, E. Segal and M. A. Krepker, in *Handbook of Porous Silicon, eds.* L. Canham, Springer 2014, pp.187-198.
3 Porous Silicon and Conductive Polymer Nanostructures Via Templating, F. A. Harraz, in *Handbook of Porous Silicon, eds.* L. Canham, Springer 2014, pp.611-622.
4 Nanostructured Polymer Blends, Sabu Thomas, Robert Shanks and C. Sarathchandran, Elsevier Inc., USA, 2014, ch. 14, pp. 495–496.
5 Y. Shi, J. Liu, and Y. Yang, *J. Appl. Phys.*, 2000, **87**, 4254.
6 A. Okada and A. Usuki, *Mater Sci Eng C*, 1995,**3**, 109.
7 W. U. Huynh, J. J. Dittmer and A. P. Alivisatos, *Science*, 2002, **295**, 2425.
8 M. M. Lee, J. Teuscher, T. Miyasaka, T. N. Murakami and H. J. Snaith, *Science,* 2012, **338**, 643.
9 K. M. Coakley, Y. Liu, M. D. McGehee, K. M. Frindell and G. D. Stucky, *Adv Funct Mater*, 2003, **13**, 301.
10 N. C. Greenham, X. Peng and A. P. Alivisatos, *Phys Rev B*, 1996, **54**, 17628.
11 D. S. Ginger and N. C. Greenham, *Synth Met.,* 1999, **101**, 425
12 K. F. Jeltsch, M. Schädel, J.-B. Bonekamp, P. Niyamakom, F. Rauscher, H. W. A. Lademann, I. Dumsch, S. Allard, U. Scherf and K. Meerholz, *Adv. Funct. Mater.*, 2012, **22**, 397.
13 J. J. Wang, J. S. Hu, Y. G. Guo and L. J. Wan, *NPG Asia Mater.*, 2012, **4**,e2.
14 E. Moons, *J. Phys. Condens. Matter*, 2002, **14**, 12235.
15 L.T. Canham, *Appl. Phys. Lett.*, 1990, **57**, 1046.
16 J.K. Mishra, S. Bhunia, S. Banerjee and P. Banerji, *J. Lumin.*, 2008, **128**, 1169.
17 V.P. Parkhutick, R. Diaz Calleja, E.S. Matveeva and J. M. Martinez-Duart, *Synth. Met.*, 1994, **67**, 111.
18 K.G. Jung, J.W. Shultze, M. Tönissen and H. Münder, Thin Solid Films, 1995, **255**, 317.
19 N. Koshida, T. Ozaki, X. Sheng and H. Koyama, *Jpn. J. Appl. Phys.*, 1995, **34**, L705.
20 N. A. Tokranova, S. W. Novak, J. Castracane and I. A. Levitsky, *J. Phys. Chem. C,* 2013, **117(44),** 22667.
21 J. W. Baltchford, S. W. Jessen, L.-B. Lin, T. L. Gustafson, D.-K. Fu, H.-L. Wang, T. M. Swager, A. G. MacDiarmid and A. J. Epstein, *Phys. Rev. B,* 1996, **54**, 9180.
22 F.A. Harraz, S.M. El-Sheikh, T. Sakka and Y.H. Ogata, *Electrochim. Acta,* 2008, **53**, 6444.
23 F.A. Harraz, A.M. Salem, B.A. Mohamed, A. Kandil and I.A. Ibrahim, *Appl. Surf. Sci.*, 2013, **264**, 391.
24 F. A. Harraz, K. Kamada, K. Kobayashi, T. Sakka, and Y. H. Ogata, *J. Electrochem. Soc.*, 2005, **152**, C213.
25 F. A. Harraz, *J. Electroanal. Chem.,* 2014, **729**, 68.
26 L. F. Marsal, P. Formentín, R. Palacios, T. Trifonov, J. Ferré-Borrull, A. Rodriguez, J. Pallarés and R. Alcubilla, *Phys. Stat. Sol.* (a), 2008, **205**, 2437.
27 P. Urbánek, I. Kuřitka, S. Daniš, J. Toušková, J. Toušek, *Polymer,* 2014, **55**, 4050.
28 M. Ram, N. Sarkar, P. Bertoncello, A. Sarkar, R. Narizzano, C. Nicolini, *Synthetic Metals,* 2001, **122,** 369.
29 F.A. Harraz, T. Sakka and Y.H. Ogata, *Electrochim. Acta,* 2001, **46**, 2805.

30 R. F. Cossiello, L. Akcelrud and T. D. Z. Atvars, *J. Braz. Chem. Soc.*, 2005, **16**, 74.
31 S. Quan, F. Teng, Z. Xu, L. Qian, Y. Hou, Y. Wang and X. Xu, *Eur. Polym. J.*, 2006, **42**, 228.
32 T.-Q. Nguyen, R. C. Kwong, M. E. Thompson and B. J. Schwartz, *J. Appl. Phys*, 2000, **76**, 2454.
33 B. Tian, G. Zerbi, R. Schenk and K. Müllen, *J. Chem. Phys.*, 1991, **95**, 3191.
34 The control of morphology and the morphological dependence of device electrical and optical properties in polymer electronics, Y. Yang, Y. Shi, J. Liu and T.-F. Guo, in *Electronic and Optical Properties of Conjugated Molecular Systems in Condensed Phases*, *eds.* S. Hotta, Research Signpost 2003, pp.307-354.
35 F. A. Harraz and A. M. Salem, *Scr. Mater.* 2013, **68**, 683.
36 D. Li, D. Yang, C. Zhou, and D. Que, *Mater. Sci. Eng. B*, 2005, **121,** 229.

Effective polymer infiltration

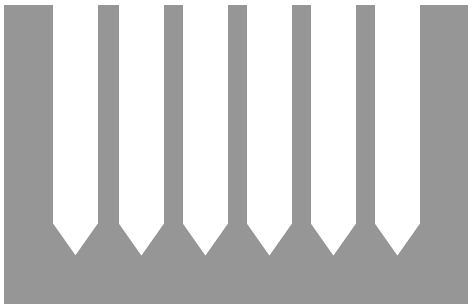

~100 nm Porous Silicon

Spin Coating

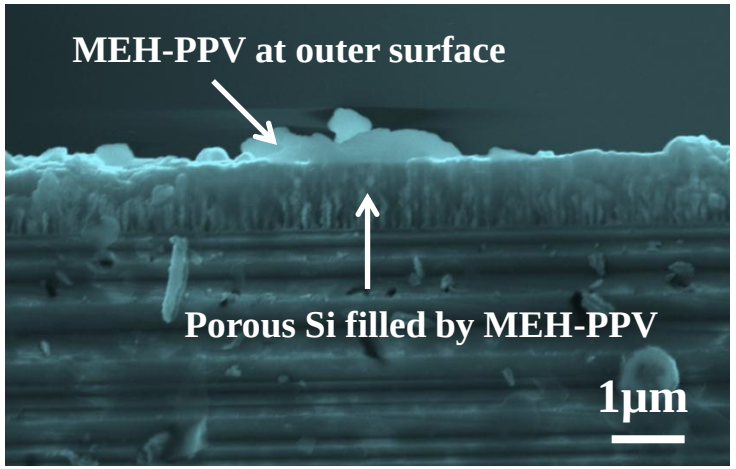

PL Enhancement